Research Article

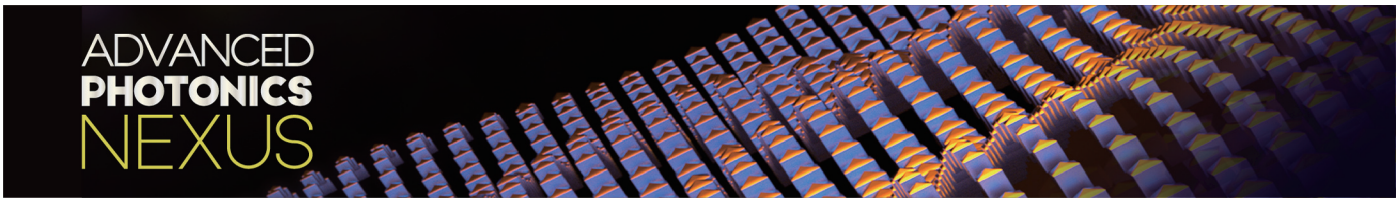

Self-mode-locking optoelectronic oscillator with ultrashort time delay

Hao Chen,[a,b,†] Shifeng Liu,[b,†] Tongtong Xie,[c] Qingshui Guo,[d] Qiuyi Shen,[a] Chen Zhu,[d] Daru Chen,[a] Hongyan Fu,[c,*] and Shilong Pan[b,*]

[a]Zhejiang Normal University, Hangzhou Institute of Advanced Studies, Hangzhou, China
[b]Nanjing University of Aeronautics and Astronautics, Ministry of Education, National Key Laboratory of Microwave Photonics, Nanjing, China
[c]Xiamen University, School of Electronic Science and Engineering, Department of Electronic Engineering, Xiamen, China
[d]Zhejiang Laboratory, Hangzhou, China

Abstract. The optoelectronic oscillator (OEO) is a typical time-delay system with rich nonlinear dynamical characteristics. Most of the previous research on OEOs has been focused on analyzing the properties of OEOs with a long time delay, which makes it difficult to realize mode locking without additional phase-locking mechanisms. We have achieved, for the first time to our knowledge, a self-mode-locking OEO and generated stable microwave frequency combs by analyzing the characteristics of OEOs with an ultrashort time scale. In the experiment, the self-mode-locking OEOs with fundamental mode, second-order harmonic, and sixth-order harmonic were realized by adjusting the system parameters, all of which produced uniform square wave signals with tunable duty cycles, steep rising and falling edges, and periods of less than 20 ns. The self-fundamental-mode-locking OEOs with different time delays were also implemented and experimentally realized. Furthermore, the experiment revealed the self-hybrid mode-locking OEO, which is the coexistence and synchronization of the three measured self-locking modes in one OEO cavity, demonstrating the complex nonlinear dynamical behaviors of the OEO system and enabling the generation of periodic nonuniform hybrid square wave signals. The realization of the self-mode-locking OEO and the generation of flexible and stable square wave signals at ultrashort time scales enrich the study of OEO nonlinear dynamics in the realm of complex microwave waveform generation, offering promising applications in areas such as atomic clocks, radars, communications, and optoelectronic neural networks.

Keywords: optoelectronic oscillator; self-mode locking; microwave frequency combs; square wave signal.

Received Feb. 19, 2024; revised manuscript received Apr. 16, 2024; accepted for publication May 23, 2024; published online Jun. 14, 2024.

[DOI: 10.1117/1.APN.3.4.046005]

1 Introduction

The optoelectronic oscillator (OEO) is a typical optoelectronic time-delay dynamical system with nonlinear, dissipative, and autonomous characteristics.[1–8] An optoelectronic feedback loop in an OEO system is normally composed of an optical branch and an electrical branch based on electrical-to-optical (E/O) and optical-to-electrical (O/E) interconversion, which can be used to generate rich and complex microwave signals with high quality.[9–11] Microwave frequency signal generation based on OEO can be broadly categorized into two main types: single-frequency microwave signal generation and complex microwave waveform generation. These signal sources find applications in a wide range of fields, including radar detection, communication, optical computing, and sensing. Without considering other complex nonlinear effects, the frequency expression for the kth oscillatory mode oscillating in the OEO is $f_k = f_0 + kc/(n_o L_o + n_e L_e)$, where f_0 is the fundamental frequency, $c/(n_o L_o + n_e L_e)$ is the free spectral range (FSR) of the oscillatory modes oscillating in the OEO, n_o and n_e are the effective refractive indices of the optical path and electrical path, respectively, and L_o and L_e are the physical lengths of the

*Address all correspondence to Shilong Pan, pans@nuaa.edu.cn; Hongyan Fu, fuhongyan@xmu.edu.cn

†These authors contributed equally to this work.

optical path and electrical path, respectively. Therefore, the OEO is a multimode oscillation cavity, with its mode spacing being the FSR. By selectively regulating the gain distribution of the internal modes of the OEO, the generation of a single-frequency microwave signal can be achieved. Numerous studies have reported the introduction of low-loss, long optical fibers as energy storage components within the OEO loop, coupled with the use of narrow-bandwidth optical or electrical filters to selectively tune the oscillation modes, thereby realizing a high-Q OEO system for generating single-frequency microwave signals with low phase noise and high quality.[12–14] To further enhance the quality of single-frequency microwave signals, improvements have been reported in OEO systems based on this foundation, such as the dual-loop OEO,[15–17] coupled OEO,[18–20] resonator-based OEO,[21,22] and electrically injected OEO.[23–25] However, the difficulties in producing narrowband optical or electrical filters, as well as their poor tunability, have hindered the development of such OEO systems. To address this issue, OEOs based on the nonlinear dynamics of semiconductor lasers[26] and OEOs based on parity-time (PT) symmetry[27–30] have been successively reported. These systems do not require optical or electrical filters within the loop and achieve a wide tunability for generating single-frequency microwave signals through the adoption of a novel and effective mode selection mechanism. The nonlinear dynamics of period-one oscillating state in semiconductor lasers with optical injection enables the generation of a wide range of single-frequency microwave signals, and combined with the optoelectronic feedback of the OEO, high-quality single-frequency microwave signals can be produced. In the PT-symmetric system, nonreal eigenvalues can be obtained through symmetry breaking induced by increasing the level of non-hermiticity, providing a new and effective approach for mode selection in OEOs.

OEOs also have unique advantages in the generation of complex microwave waveforms. Many types of OEOs have been successively reported to generate complex microwave waveforms, such as Fourier-domain mode-locked OEOs,[31,32] active mode-locked OEOs,[33,34] passive mode-locked OEOs,[35,36] parametric OEOs,[37] random OEOs,[38,39] soliton OEOs,[40] and chaotic OEOs.[41,42] In the Fourier-domain mode-locked OEO, a single-chirp linear frequency-modulated (LFM) microwave waveform is realized by adjusting the period of the linear swept frequency source to match the oscillation delay of the OEO loop, forming Fourier-domain mode locking in the OEO oscillation loop. By shaping the swept frequency filter in the OEO loop, dual-chirp LFM microwave waveforms, complementary LFM microwave waveforms, phase-coded microwave waveforms, and other complex microwave waveforms are generated. The basic principle of the active mode-locked OEO is to inject external microwave signals into the OEO loop, whose microwave signal period matches the delay of the OEO loop, making the OEO cavity phase-locked between the injected signal and the oscillating modes of the OEO, thus realizing the generation of stable microwave pulses and microwave frequency combs (MFCs). It can realize the generation of many types of complex microwave signals through the design of the injected microwave signals in terms of frequency, waveform, and other parameters. In the passive mode-locked OEO, an ultranarrow single-cycle microwave pulse is realized using a saturable radio frequency (RF) amplifier as a mode-locked device in the loop, without any external microwave signal injection. The parametric OEO can realize the phase locking of the modes in the OEO cavity to form mode-locked oscillations using an electrical mixer as a phase control unit. Random-signal OEOs enable the generation of random microwave signals without time delay using specially fabricated optical fibers as part of the OEO loop for random distributed feedback of the optical signals, which is equivalent to the simultaneous oscillation of multiple OEOs with different loop lengths. A dissipative soliton OEO achieves a nonlinear gain saturation effect through the interaction between two modes by introducing a double-pass band filter in the cavity and reaches a steady state with the linear filtering effect, thus realizing the generation of microwave photonic dissipative soliton and frequency-hopping microwave signals. The principle of chaotic OEO is that the nonlinear dynamical state of OEO evolves from a breathing state to a chaotic state when the cavity gain is gradually increased, generating a broadband chaotic microwave signal. All of the OEO structures reported above can be classified as long-time delay-based OEOs because long-distance optical fibers are used in the loops; however, short-time delay-based OEOs and their nonlinear dynamics have rarely been reported.

In this paper, an ultrashort-time-delay-based OEO is proposed and experimentally demonstrated, which leverages its short-cavity characteristics to achieve significant benefits. It presents the first demonstration of a self-mode-locking state in an OEO structure utilizing an ultrashort time delay. This configuration produces a wideband MFC, characterized by a high-quality periodic square-wave signal with a tunable duty cycle and a period of $T = 1/\mathrm{FSR}$. Furthermore, by adjusting system parameters, the ultrashort time-delay-based OEO achieves the interswitching between the fundamental mode self-locking state and the higher-order harmonic self-locking state within the OEO cavity. This transition is observed as a square-wave pulse splitting with a period of $T = (1/N) \times (1/\mathrm{FSR})$, where N is the order of the harmonic. In addition, a hybrid self-mode-locking state, where the fundamental mode self-locking state and the higher-order harmonic self-locking state coexist, is discovered using the ultrashort time-delay-based OEO structure. The time-domain waveform of the hybrid signal exhibits a periodic nonuniform square wave, resulting from the mutual coupling of the amplitude of square wave signals from both locking states with a period of $T = 1/\mathrm{FSR}$. In the experiment, stable MFCs with a large bandwidth of 20 GHz were generated, all of which produced high-quality uniformly shaped square wave signals in the time domain with tunable duty cycles, steep rising and falling edges, and periods of <20 ns. The self-fundamental mode-locking OEOs with different loop lengths of 3.4, 5.5, and 27.8 m were realized. Furthermore, the experiment revealed the coexistence of these three self-locking modes, showcasing the complex nonlinear dynamical behaviors of the OEO system and enabling the generation of abundant periodic nonuniform square wave signals. The realization of self-mode-locking OEOs and the generation of flexible and stable square wave signals at ultrashort time scales enrich the study of OEO nonlinear dynamics in the realm of complex microwave waveform generation, offering promising applications in areas such as atomic clocks, radars, communications, and optoelectronic neural networks.

2 Principle

The schematic diagram of the proposed self-mode-locking OEO with ultrashort time delay is shown in Fig. 1(a), which is focused on the generation of stable MFCs; the illustration of the corresponding abundant time-domain square signals is shown in

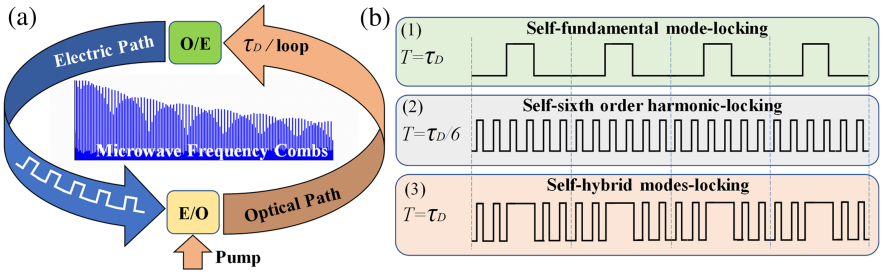

Fig. 1 (a) The schematic diagram of the proposed self-mode-locking OEO with ultrashort time delay and (b) the illustration of the generated time-domain square wave signals.

Fig. 1(b). The proposed OEO structure consists of a pump laser and a hybrid microwave photonic cavity, which is a typical optoelectronic time-delay system, in which the optical signal and electrical signal are converted to each other using an electro-optic modulator and a photodetector (PD). The optoelectronic time-delay systems have been widely investigated to possess rich and complex dynamic characteristics, such as relaxation oscillation, chaotic breathing, and a high-dimensional chaos state, by analyzing the delay differential equation (DDE) or the evolution version from the Ikeda theoretical model. In this configuration, no optical or electrical filter is used in the OEO cavity, so the bandpass filtering effect of the OEO loop is only determined by the bandwidth of the devices in the cavity. The theoretical model of the proposed OEO can be equivalent to a broad bandpass filter-based OEO, and the Ikeda-like DDE can be written as

$$x(t)+\tau\frac{dx(t)}{dt}+\frac{1}{\theta}\int_0^t x(s)\mathrm{d}s=\beta\{\cos^2[x(t-\tau_D)+\phi]-\cos^2(\phi)\}, \tag{1}$$

where the integral time $\tau=1/2\pi f_H$ and the differential time $\theta=1/2\pi f_L$ are related to the bandpass filter with a low cut-off frequency of f_L and a high cut-off frequency of f_H.$x(t)=\pi V(t)/2V_\pi$ is the dimensionless variable of the generated microwave signal in the OEO cavity. $V(t)$ is the electrical voltage generated from the PD, and V_π is the RF half-wave voltage of the modulator. τ_D is the time delay of the OEO loop. The normalized parameter $\beta=\gamma RGAP_0\pi/2V_\pi$ is the normalized gain coefficient of the delayed loop, and γ and R are the responsivity and the output matching resistance of the PD, respectively. G is the gain of the low noise amplifier (LNA), A is the overall loss of the OEO loop, and P_0 is the optical power of the pump laser. $\varphi=\pi V_{\mathrm{Bias}}/2V_{\pi 0}$ is the offset phase of the modulator with a direct current (DC) half-wave voltage of $V_{\pi 0}$, which is biased with the voltage V_{Bias}. By introducing an integral term as

$$y(t)=\int_0^t x(t)\mathrm{d}t. \tag{2}$$

Equation (1) can be rewritten as

$$\begin{cases}\dfrac{dx(t)}{dt}=-\dfrac{1}{\tau}x(t)-\dfrac{1}{\tau\cdot\theta}y(t)+\dfrac{\beta}{\tau}\{\cos^2[x(t-\tau_D)+\phi]-\cos^2(\phi)\}\\ \dfrac{dy(t)}{dt}=x(t),\end{cases} \tag{3}$$

where Eq. (3) is a typical modified Ikeda-like equation. Rich dynamic characteristics can be realized by tuning the bias voltage V_{Bias} and the gain coefficient of the OEO loop. To simplify the simulation and make it close to the experimental parameters, the time delay τ_D of the self-mode-locking OEO is set as 20 ns, the normalized gain coefficient β is set as 1.2, and the low and high cut-off frequencies are set as 50 kHz and 10 GHz, respectively. The variable offset phase φ can be tuned by changing the biased voltage V_{Bias} of the modulator with a DC half-wave voltage $V_{\pi 0}$ of 4.0 V. In the simulation result, time-domain square wave signals with the same period T of 20 ns ($T=\tau_D$) are generated with different phases ϕ, where the simulation results are shown in Fig. 2. In Fig. 2, as the phase is tuned from −0.985 to −0.585 with a step of 0.2, the duty cycle of the square wave is increased from 0.34 to 0.45 and 0.65, respectively. The periods of the square wave signals are the same as the setting value of the time delay of the OEO loop. It means that broad bandpass filter OEOs can realize periodic oscillations with the same time delay of the OEO loop by setting the system parameters under an ultrashort time delay.

Mode-locking technology in ring-cavity fiber lasers has been well established,[43,44] but self-mode-locking oscillation has not yet been achieved in OEO structures due to the limitations of long fiber and filter used in the loop, which is due to the inability of the intraring cavity gain to meet the phase locking of all modes in the cavity. According to the mode-selection mechanism in the ring cavity, the short-cavity-based OEO (several meters) has 3 orders of magnitude fewer modes oscillating than the number of modes in the long-cavity-based OEO (several kilometers) in the same microwave frequency range. Therefore, with the same loop gain condition, each mode of the short-cavity-based OEO can obtain a larger gain, which results in the formation of self-excited oscillations within the OEO cavity. On the other hand, since no filter is used in the short-cavity-based OEO, each mode in the loop is formed by the superposition of several different modulated harmonic components due to the nonlinear effects of the modulator, where the periods of the individual harmonics are multiplicatively related. By fine-tuning the bias voltage of the modulator, the phase of the harmonic components is changed, and phase locking between the harmonic components in one mode can be achieved under certain conditions, so that the phases between different harmonics-combined modes are also locked, thus achieving a self-mode-locking state and generating a stable MFC. Therefore, there are two main factors for the formation of the self-mode-locking state; one is that the OEO cavity has sufficient gain to each oscillating mode, and the other is that the phase coherence of the oscillating modes can be realized. What is more, the same as with the pulse splitting

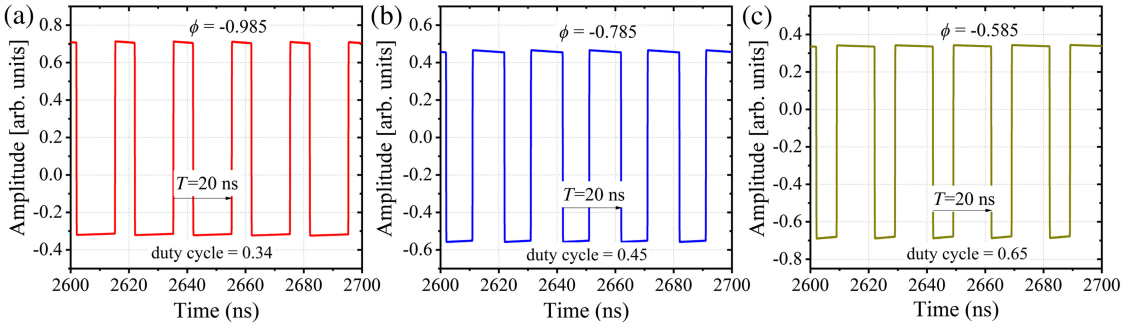

Fig. 2 The simulation results of the square-wave signals with different duty cycles under different phases. (a) $\phi = -0.985$, (b) $\phi = -0.785$, and (c) $\phi = -0.585$.

phenomenon in mode-locking fiber lasers, under the influence of power and nonlinearities, the square-wave pulses of the self-mode-locking OEO can be split, and mutual attraction and repulsion occur between the split multiple pulses. A stable harmonic-mode-locking pulse output can be formed when the time interval of the multiple pulses is exactly one integer fraction of the time interval of the round trip in the OEO cavity. Therefore, the period of the square wave signal changes from τ_D to τ_D/N, where N is the order of harmonics. Figures 1(b-1) to 1(b-2) show the illustration of the time-domain square wave in the self-fundamental-mode-locking state spilled to the self-sixth-order harmonic-locking state, where the period of the square wave is switched from τ_D to $\tau_D/6$.

Under certain conditions, there may be simultaneous mode-locked oscillations of the fundamental mode and high-order harmonics in one mode-locked cavity, forming a hybrid mode-locking state. Usually, the time-domain waveform of the mode-locked system is a Gaussian pulse with an ultranarrow pulse width in the mode-locked fiber laser structures, and it is difficult to observe the hybrid mode-locking state because the pulse periods generated by different mode-locked modes are integer multiples of each other. In the self-mode-locking OEO cavity, since the generated time-domain signal is a periodic square wave signal with a tunable duty cycle, the hybrid mode-locking state can be analyzed intuitively by observing the combined superposition state of the square waves generated by different mode-locked modes. Figure 1(b-3) shows the illustration of the time-domain signals with a hybrid mode-locking state of the square waves with the self-fundamental mode-locking state in Fig. 1(b-1) and self-sixth-order harmonic-locking state in Fig. 1(b-2). In this case, the low-level region of the square wave with the self-fundamental mode locking is occupied by the square wave with the self-sixth-order harmonic locking; the high-level region is not occupied. Hence, forming a periodic nonuniform square waveform whose period is equal to the period of the square wave with self-fundamental mode locking, i.e., the time delay of the OEO, τ_D.

3 Experimental Results

The experimental structure of the self-mode-locking OEO with ultrashort time delay is shown in Fig. 3. A pump beam with a central wavelength of 1550.0 nm and an optical power of 16.0 dBm is injected into the OEO loop through a polarization controller (PC) and a Mach–Zehnder modulator (MZM, iXblue MXAN-LN-10). The OEO loop is composed of an MZM, a PD (3-dB bandwidth: 18 GHz), an LNA (band: 50 kHz to 20 GHz,

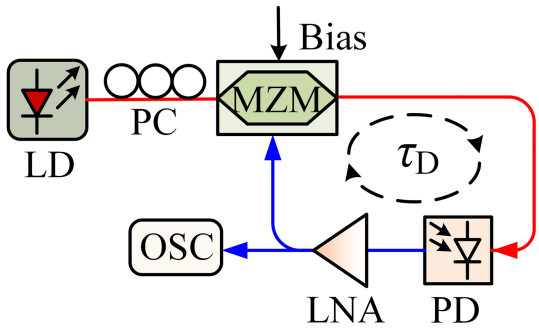

Fig. 3 The experimental structure of the self-mode-locking OEO with ultrashort time delay.

gain: 30 dB), and an electrical power divider. It is worth noting that the tail fiber of the MZM is directly connected to the tail fiber of the PD, so the length of the entire OEO loop is about 3.0 m. A real-time oscilloscope (OSC, KEYSIGHT UXR0594A, 59 GHz, 250 GSa/s) is used to synchronously detect the electrical frequency spectrum and the corresponding time-domain waveform.

3.1 Self-Fundamental Mode-Locking OEO with a Period of τ_D

In the experiment, by adjusting the parameters of the proposed OEO system in Fig. 3, a self-mode-locking OEO can be realized, which can produce stable MFCs, and the corresponding time-domain signals present rich square-wave waveforms. As the V_{Bias} of the MZM is set at 0.6 V, a self-fundamental-mode-locking state is realized, where an MFC is generated and the corresponding time-domain signal is a periodic square waveform, as shown in Fig. 4(a). In Fig. 4(a-i), the generated MFC shows a large bandwidth from 0 to 20 GHz and an FSR of 60 MHz. The signal-to-noise ratio (SNR) of the MFC with a range from 0 to 4.0 GHz can be up to 40 dB. Figure 4(a-ii) shows the corresponding time-domain waveform, which is a classical square waveform with a period T of 16.8 ns. The rising and falling times of the generated square waveform are about 60.3 and 85.2 ps, respectively. The duty factor of the generated square wave signal is 0.30. The period of the generated square wave is matched with the time delay τ_D of the OEO loop, and the length of the OEO loop can be calculated as 3.4 m. Increasing the value of the V_{Bias} from 0.6 to 4.8 V, the proposed OEO system still keeps the self-fundamental mode-locking state

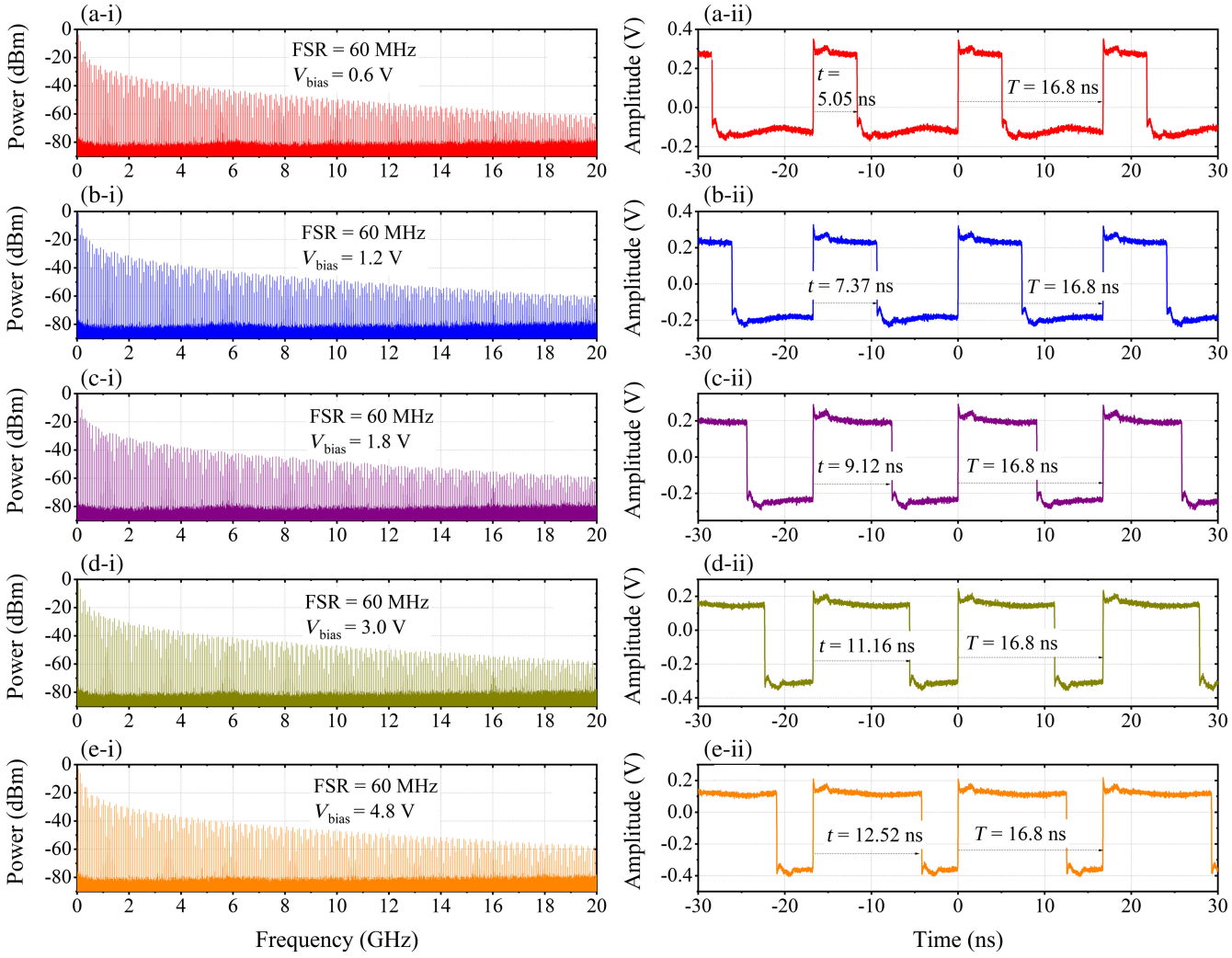

Fig. 4 The MFCs (left columns) and corresponding time-domain square waves (right columns) generated by self-fundamental-mode-locking OEO with different bias voltages V_{Bias} in the MZM. (a) V_{Bias} = 0.6 V, (b) V_{Bias} = 1.2 V, (c) V_{Bias} = 1.8 V, (d) V_{Bias} = 3.0 V, and (e) V_{Bias} = 4.8 V.

in the experiment. Some selected MFCs with different bias voltages (1.2, 1.8, 3.0, and 4.8 V) are shown in Figs. 4(b)–4(e), respectively. All of the MFCs generated in Fig. 4 have the same FSR, and the corresponding time-domain signal is a square-wave signal with the same period T of 16.8 ns, which means that the proposed OEO is kept as a self-fundamental-mode-locking state. Interestingly, different bias voltages result in different overall power distributions of the generated MFCs, which causes the duty cycle of the corresponding square wave to change. From Figs. 4(b-ii)–4(e-ii), the duty cycles of the generated square-wave signals are increased to 0.44, 0.54, 0.66, and 0.75, respectively. This means that the proposed self-fundamental-mode-locking OEO can generate stable MFCs with the same FSR and square waveforms with the same periodic and tunable duty cycle.

3.2 Self-Second-Order Harmonic-Locking OEO with a Period of $\tau_D/2$

It is found in the experiment that the proposed self-mode-locking OEO system can evolve from the self-fundamental-mode-locking state to the self-harmonic-locking state with the same OEO loop. Figure 5 shows the experimental results of the self-second-order harmonic-locking OEO for generating MFCs and the corresponding time-domain waveforms with different V_{Bias}. All of the MFCs in Fig. 5 have the same FSR of 120 MHz, which is twice that in Fig. 4. The SNR of the generated MFCs in Fig. 5 is much better than that in Fig. 4, which is about 40 dB, with a range from 0 to 8.0 GHz. This is because under the same loop gain condition, the number of frequency combs generated by the harmonic-locking OEO is less than that in a self-fundamental mode-locking OEO, so the gain of each comb tooth is larger. The time-domain signals in Fig. 5 are periodic uniform square waves with the same period and tunable duty cycles, which is similar to that in a self-fundamental-mode-locking OEO. The period of the square waves in Fig. 5(b) is 8.3 ns, which is half of that in Fig. 4. As the V_{Bias} is tuned from 11.8 to 13.4 V with a step of 0.4 V, the duty cycle of the corresponding square wave signal is 0.41, 0.47, 0.51, 0.55, and 0.59 V, respectively. The rising and falling times of the generated square waveforms are <100 ps.

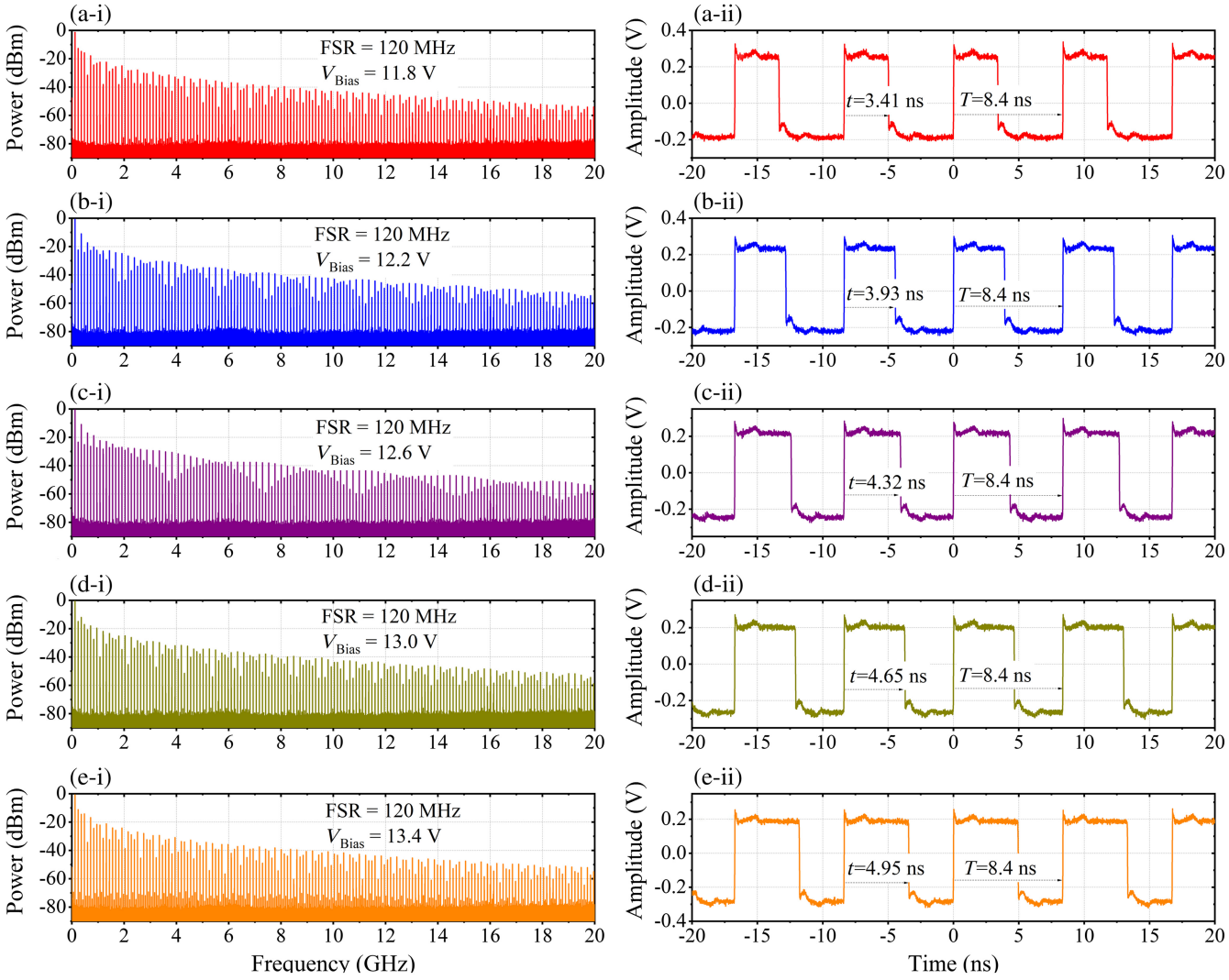

Fig. 5 The MFCs (left columns) and corresponding time-domain square waves (right columns) generated by self-second-order harmonic-locking OEO with different bias voltages V_{Bias} in the MZM. (a) $V_{Bias} = 11.8$ V, (b) $V_{Bias} = 12.2$ V, (c) $V_{Bias} = 12.6$ V, (d) $V_{Bias} = 13.0$ V, and (e) $V_{Bias} = 13.4$ V.

3.3 Self-Sixth-Order Harmonic-Locking OEO with a Period of $\tau_D/6$

By adjusting the polarization state of the pump source, the proposed OEO system also realizes a self-sixth-order harmonic-locking OEO, which generates an MFC with an FSR of 360 MHz, whose corresponding time-domain signal is a homogeneous square wave with a period of 2.8 ns. The duty cycle of the square wave is tunable under different bias voltage conditions; the experimental results are shown in Fig. 6. The MFCs generated in Fig. 6 show the same FSR of 360 MHz, which is 6 times that in Fig. 4. Uniform square waves with a period of 2.8 ns are generated, which is one-sixth of τ_D. From Figs. 6(b-ii)–6(e-ii), the duty cycle of the generated square waves is increased from 0.3 to 0.54 as the V_{Bias} is tuned from 0.5 to 2.0 V. The experimental results from Figs. 4–6 show that the proposed self-mode-locking OEO can realize self-fundamental mode-locking and self-high-order harmonic-locking states, and the time-domain square wave signals of the generated MFCs with different FSRs have different periods and tunable duty cycles.

3.4 Signal Quality of the Generated MFCs in the OEO with Different Self-Mode-Locking States

In the experiment, the phase noise of the different fundamental frequencies in the MFCs generated in the self-fundamental mode-locking OEO, the self-second-order harmonic-locking OEO, and the self-sixth-order harmonic-locking OEO are measured, as shown in Fig. 7. Since there is no long optical fiber as an energy storage element in the loop of the self-mode-locking OEO with an ultrashort time delay, the signal quality of the generated MFC is inferior compared to that of the OEO with a long optical fiber for the single-frequency microwave signal generation. In Fig. 7, as the fundamental frequencies of the MFCs are 60, 120, and 360 MHz, the corresponding phase noises are 109 dBc/Hz@10 kHz, 103 dBc/Hz@10 kHz, and 95 dBc/Hz@10 kHz, respectively.

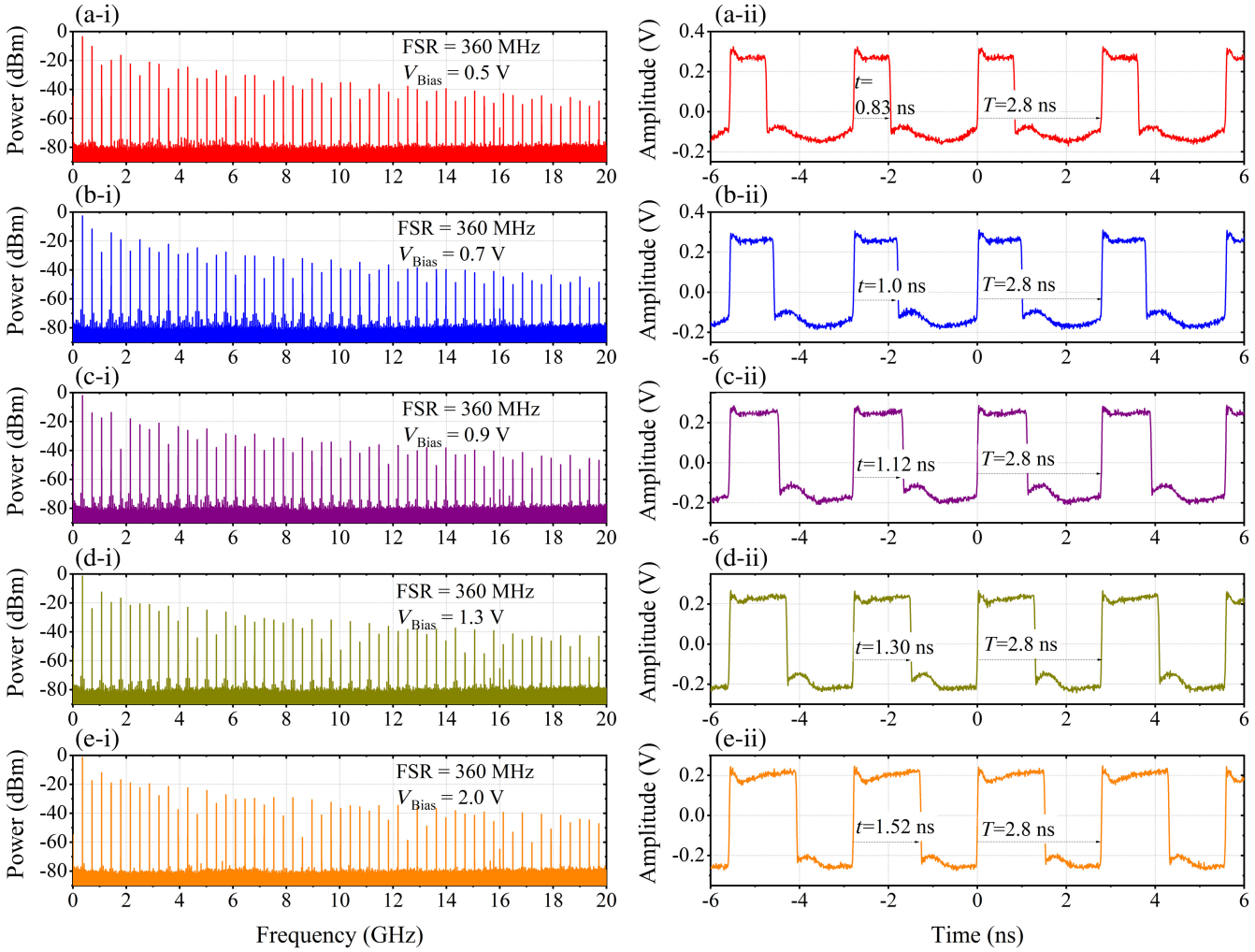

Fig. 6 The MFCs (left columns) and corresponding time-domain square waves (right columns) generated by self-sixth-order harmonic-locking OEO with different bias voltages V_{Bias} in the MZM. (a) V_{Bias} = 0.5 V, (b) V_{Bias} = 0.7 V, (c) V_{Bias} = 0.9 V, (d) V_{Bias} = 1.3 V, and (e) V_{Bias} = 2.0 V.

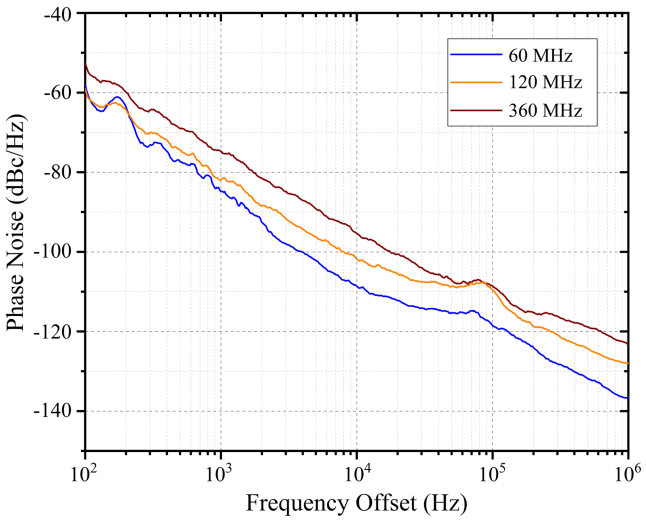

Fig. 7 The measured phase noises of the fundamental frequency of the MFCs with different FSRs (blue line, 60 MHz; orange line, 120 MHz; and brown line, 360 MHz).

3.5 Self-Mode-Locking OEOs with Different Time Delays

As a comparison, self-fundamental-mode-locking OEOs with different time delays are realized in the experiment by adding optical fibers with different lengths, as shown in Fig. 8. In Fig. 8(a-i), a self-fundamental-mode-locking MFC with a bandwidth from 0 to 20 GHz and an FSR of 60 MHz is generated, and the inset diagram in Fig. 8(a-i) is part of the MFC from 0 to 3.0 GHz. The corresponding time-domain square-wave signal with a period of 16.8 ns is shown in Fig. 8(a-ii), which matches the time delay of the OEO loop. As the length of the OEO loop is tuned to 5.5 m, an MFC with the same frequency range and an FSR of 36.6 MHz is generated, as shown in Fig. 8(b-i), and the inset diagram in Fig. 8(b-i) is part of the generated MFC from 0 to 2.0 GHz. The corresponding time-domain signal is shown in Fig. 8(b-ii); it is a periodic square-wave signal with a period of 27.26 ns, which is matched with the time delay of the OEO loop. Finally, the length of the OEO is tuned to 27.8 m; the self-fundamental-mode-locking OEO is also realized by appropriately adjusting the polarization state and bias voltage of the OEO system, as shown in Fig. 8(c). An MFC with an FSR of

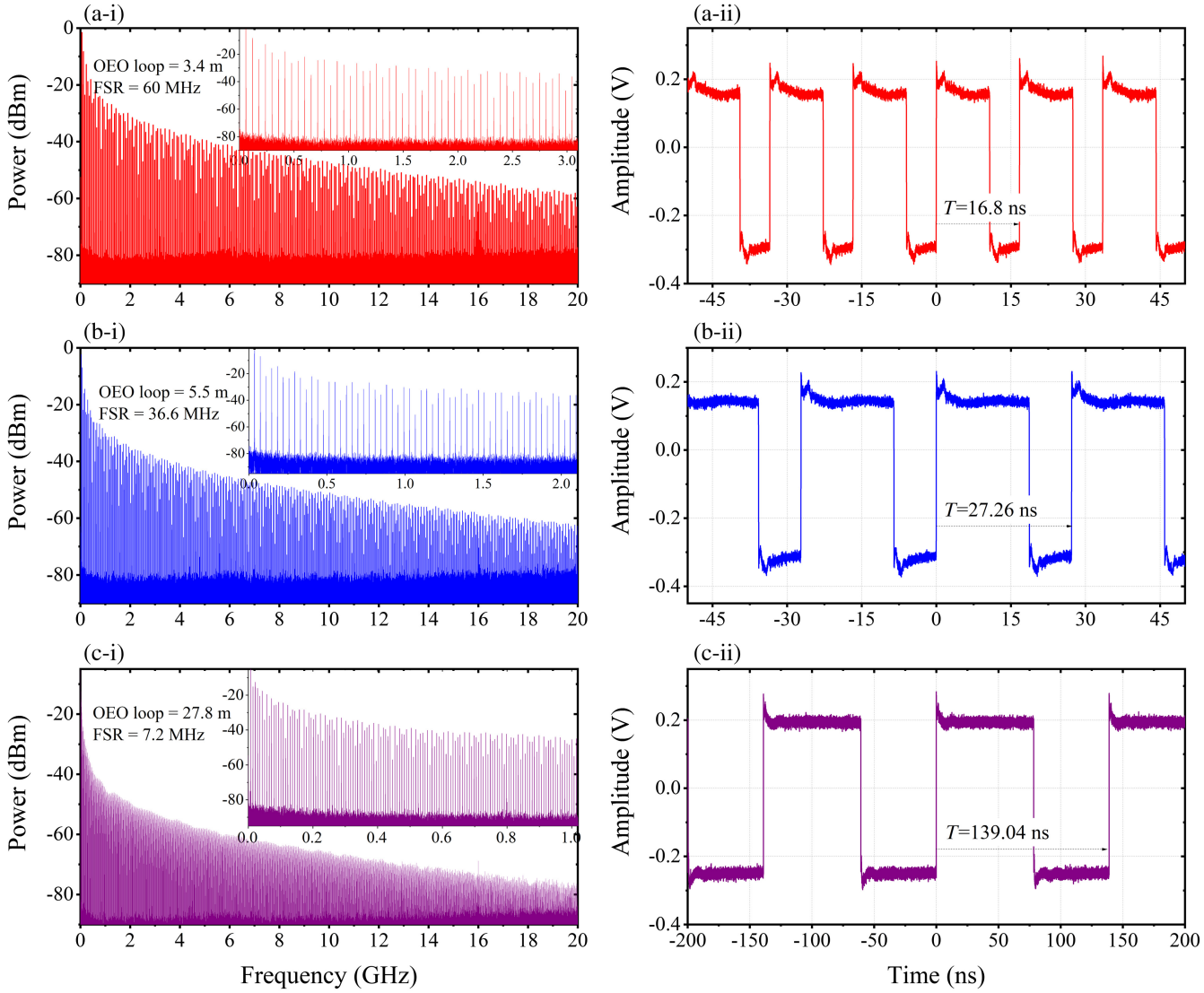

Fig. 8 The MFCs (left columns) and corresponding time-domain square waves (right columns) generated by self-fundamental-mode-locking OEOs with different loop lengths. (a) OEO loop is 3.4 m, (b) OEO loop is 5.5 m, and (c) OEO loop is 27.8 m.

7.2 MHz is generated in Fig. 8(c-i), where the inset diagram in Fig. 8(c-i) is part of the generated MFC from 0 to 1.0 GHz. Figure 8(c-ii) shows the measured time-domain signal of the OEO, which is a square-wave signal with a period of 139.04 ns. It is the same as the time delay of the OEO loop.

3.6 Self-Hybrid Mode-Locking OEO with a Period of τ_D

With the change of bias voltage and the polarization state of the light, the nonlinear dynamic characteristics in an OEO show more complex forms. The periodic uniform square-wave signal can evolve into the periodic nonuniform square-wave signal, as shown in Fig. 9. In Fig. 9, 12 nonuniform square waveforms with the same period of 16.8 ns are detected in the experiment, which is equal to the time delay, τ_D, of the OEO loop. Nonuniform square waves are formed due to the simultaneous existence of three different situations of self-mode-locking states with stable oscillations in the OEO cavity and the inconsistency in the period of the square waves generated by the three oscillations. By adjusting the OEO system parameters, the strength and duty cycle of the three uniform square waves are changed, resulting in a variety of rich nonuniform square waves in Fig. 9. Among these nonuniform square waveforms, they can be categorized into six groups according to the pattern of high and low levels in the square waveforms, which are shown in Figs. 9(a-i) and 9(a-ii), Figs. 9(b-i) and 9(b-ii), Figs. 9(c-i) and 9(c-ii), Figs. 9(d-i) and 9(d-ii), Figs. 9(e-i) and 9(e-ii), and Figs. 9(f-i) and 9(f-ii). For example, in Figs. 9(a-i) and 9(a-ii), two periodic nonuniform square-wave signals with opposite electrical levels are generated, and the other groups follow a similar pattern. That means the phase shift of the generated nonuniform square-wave signal can be tuned to a paradoxical state.

From Fig. 9, it can be observed that the resulting nonuniform square wave measured in the experiment is a superposition of three uniform square-wave states generated by the self-fundamental-mode locking, the self-second-order harmonic-locking, and the sixth second-order harmonic-locking states. Figure 10

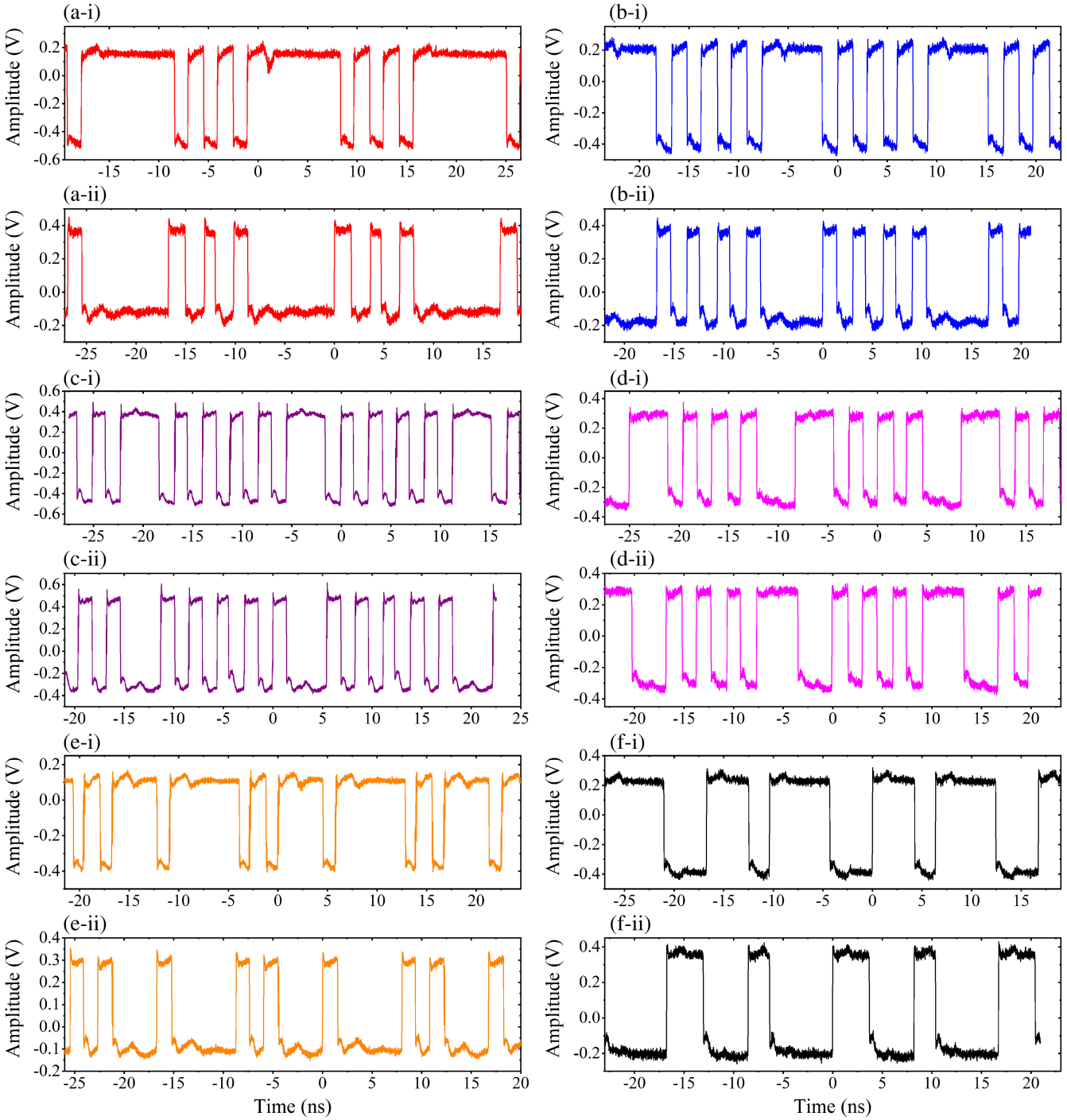

Fig. 9 The measured periodic nonuniform square-wave signals.

shows the composition analysis of parts of the nonuniform square waves measured in Fig. 9. The nonuniform square wave in Fig. 9(a-i) has the same period as the uniform square wave under the self-fundamental mode-locking state, and the nonuniform square wave in one period is composed of two kinds of square waves, which are square waves under the self-fundamental mode-locking state and the self-sixth-order harmonic-locking state. The analysis is shown in Fig. 10(a). The red line, green line, and purple line in Fig. 10(a) represent the self-fundamental mode-locking square wave, the self-sixth-order harmonic-locking square wave, and the hybrid square wave, respectively. It can be seen that under the condition that both the self-fundamental mode-locking (first) square wave and the self-sixth-order harmonic-locking (sixth) square wave exist in the OEO cavity, as the level of the first square wave is "1" (high level), the waveform of the hybrid square wave is consistent with that of the first square wave; when the level of the first square wave is "0" (low level), the waveform of the hybrid square wave is consistent with that of the sixth square wave. The pattern of square waveform-electrical level variation is

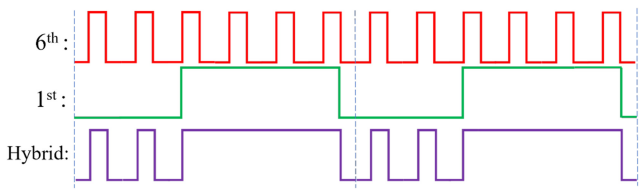

Square wave	Electrical level	Electrical level
6th:		
1st:	1	0
Hybrid:	1st wave	6th wave

(a)

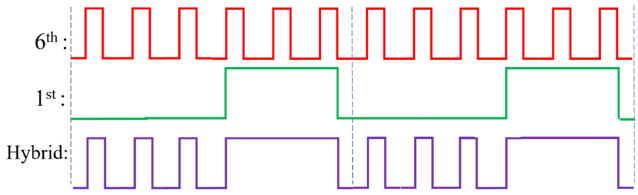

Square wave	Electrical level	Electrical level
6th:		
1st:	1	0
Hybrid:	1st wave	6th wave

(b)

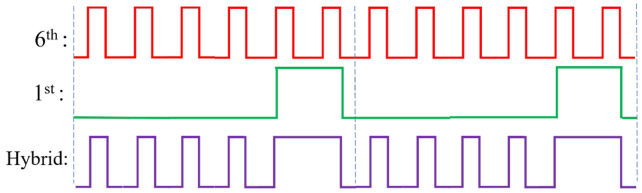

Square wave	Electrical level	Electrical level
6th:		
1st:	1	0
Hybrid:	1st wave	6th wave

(c)

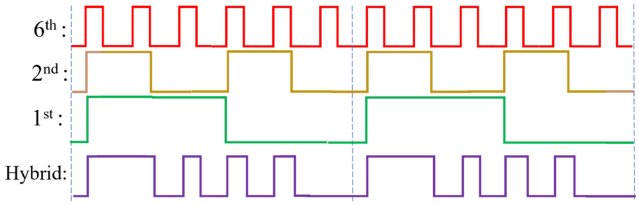

Square wave	Electrical level	Electrical level	Electrical level	Electrical level
6th:				
2nd:	1	0	1	0
1st:	1	1	0	0
Hybrid:	1st wave	6th wave	6th wave	1st wave

(d)

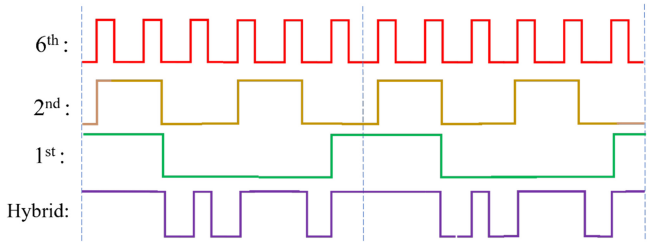

Square wave	Electrical level	Electrical level	Electrical level	Electrical level
6th:				
2nd:	1	0	1	0
1st:	1	1	0	0
Hybrid:	1st wave	1th wave	2th wave	6st wave

(e)

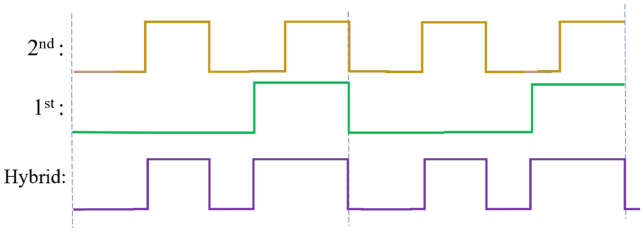

Square wave	Electrical level	Electrical level	Electrical level	Electrical level
6th:				
2nd:	1	0	1	0
1st:	1	1	0	0
Hybrid:	1st wave	1th wave	2th wave	2st wave

(f)

Fig. 10 The composition analysis of the nonuniform square waves measured in Fig. 9. (a) Fig. 9(a-i), (b) Fig. 9(b-i), (c) Fig. 9(c-i), (d) Fig. 9(d-i), (e) Fig. 9(e-i), and (f) Fig. 9(f-i).

shown in the table of Fig. 10(a). Figures 10(b) and 10(c) show the waveform composition analysis in Figs. 9(b-i) and 9(c-i), respectively, which has the same pattern as that in Fig. 10(a); just the duty cycle of the first square wave changes. Figure 10(d) shows the analysis of the hybrid square wave measured in Fig. 9(d-i). Unlike the previous three hybrid square waves, the hybrid square wave in Fig. 9(d-i) is formed by combining the first square wave, the second square wave, and the sixth square wave, and the combination mode is also more abundant. With the condition that the first square wave is "1," as the second square wave is "1," the hybrid square wave has the same square waveform as the first square wave; as the second square wave is "0," the hybrid square wave has the same square waveform as the sixth square wave. Under the condition that the first square wave is "0," when the second square wave is "1," the hybrid square wave shows the same waveform as the sixth square waveform; when the second square wave is "0," the hybrid square wave is the first square waveform. The table in Fig. 10(d) shows the law of the hybrid square waveform with the variation of the electrical level. The reasons for the different hybrid square waves are complex, the main ones being the relative time delay, duty cycle, and power of the different period square waves. Matching of several parameters can realize stable and rich hybrid square waveforms. Figure 10(e) shows another hybrid square waveform measured in Fig. 9(e-i), which is composed of the first square wave, the second square wave, and

the sixth square wave. When the electrical level of the first square wave is "1," the electrical level of the hybrid square wave is consistent with the first square wave; as the electrical level of the first square wave is "0" and the electrical level of the second square wave is "1," the waveform of the hybrid square wave is consistent with the second square wave; otherwise, it is consistent with the sixth square waveform. Finally, we analyze the waveform composition of the hybrid square wave measured in Fig. 9(f-i), as shown in Fig. 10(f). The hybrid square wave is a combination of the first square wave and the second square wave, and the waveform of the hybrid square wave is consistent with the first square wave when the electrical level of the first square wave is "1"; the waveform of the hybrid square wave is consistent with the waveform of the second square wave as the electrical level of the first square wave is "0." With the experimentally measured various hybrid square waveforms in Fig. 9 and the analysis of their square wave compositions in Fig. 10, the self-mode-locking OEO can synchronize a variety of self-mode-locking patterns. By adjusting the system parameters and controlling the relative power, phase, and relative time delay of different self-mode-locking states, rich hybrid square waveforms can be realized.

4 Conclusion

In this paper, a self-mode-locking OEO with an ultrashort time delay is proposed and experimentally demonstrated. Due to the ultrashort cavity length of the OEO loop and the absence of a filter used in the proposed OEO, the oscillation modes in the OEO cavity gain enough to form a self-mode-locking state. Stabilized MFCs with large bandwidths and corresponding time-domain periodic square waves with tunable duty cycles, ultranarrow rising and falling edges, and the same period as the time delay of the OEO loop can be generated, which causes a self-fundamental-mode-locking OEO. By tuning the bias voltage of the MZM, the self-fundamental-mode-locking state can be switched to a self-harmonic-locking state in the same OEO structure. In addition to this, different self-mode-locking states can coexist in one OEO cavity and form a steady-state competition, resulting in a periodic nonuniform square wave. In the experiment, self-fundamental-mode-locking, self-second-order harmonic-locking, and self-sixth-order harmonic-locking OEOs with the same OEO loop of 3.4 m are, respectively, realized, where the FSRs of the generated MFCs are 60, 120, and 360 MHz, and the period of the corresponding time-domain square waves is 16.8, 8.6, and 2.8 ns, respectively. Three different OEO cavity lengths of 3.4, 5.5, and 27.8 m are also set up in the experiment to realize the self-fundamental-mode-locking OEO, respectively. In addition to this, by adjusting the system parameters, stable hybrid oscillations of self-fundamental-mode-locking, self-second-order harmonic-locking, and self-sixth-order harmonic-locking states in the OEO cavity are also achieved in the experiment, reflected in the shape of the square wave as periodic nonuniform square waveforms. Twelve rich nonuniform square waves are realized in the experiment by adjusting the strength and delay of three self-mode-locking states. The realization of self-mode-locking OEO and the generation of flexible and stable square wave signals at ultrashort time scales enrich the study of OEO nonlinear dynamics in the realm of complex microwave waveform generation, offering promising applications in areas such as atomic clocks, radars, communications, and optoelectronic neural networks.

Disclosures

The authors declare no competing financial interests.

Code and Data Availability

Data underlying the results presented in this paper are not publicly available at this time but may be obtained from the authors upon reasonable request.

Acknowledgments

This work was supported by the National Natural Science Foundation of China (Grant No. 62301495) and the Project of the National Key Laboratory of Microwave Photonics (Nanjing University of Aeronautics and Astronautics), Ministry of Education (Grant No. NJ20220007).

References

1. Y. K. Chembo et al., "Chaotic breathers in delayed electro-optical systems," *Phys. Rev. Lett.* **95**(20), 203903 (2005).
2. Y. K. Chembo et al., "Nonlinear dynamics and spectral stability of optoelectronic microwave oscillators," *IEEE J. Quantum Electron.* **44**(9), 858–866 (2008).
3. M. Peil et al., "Routes to chaos and multiple time scale dynamics in broadband bandpass nonlinear delay electro-optic oscillators," *Phys. Rev. E* **79**(2), 026208 (2009).
4. K. E. Callan et al., "Broadband chaos generated by an optoelectronic oscillator," *Phys. Rev. Lett.* **104**(11), 113901 (2010).
5. L. Maleki, "The optoelectronic oscillator," *Nat. Photonics* **5**(12), 728–730 (2011).
6. L. Weicker et al., "Strongly asymmetric square waves in a time-delayed system," *Phys. Rev. E* **86**(5), 055201 (2012).
7. L. Laurent, "Complexity in electro-optic delay dynamics: modeling, design and applications," *Philos. Trans. R. Soc. A* **371**(1999), 20120464 (2013).
8. Y. K. Chembo et al., "Optoelectronic oscillators with time-delayed feedback," *Rev. Mod. Phys.* **91**(3), 035006 (2019).
9. T. F. Hao et al., "Recent advances in optoelectronic oscillators," *Adv. Photonics* **2**(4), 044001 (2020).
10. M. Li et al., "Tutorial on optoelectronic oscillators," *APL Photonics* **6**(6), 061101 (2021).
11. T. F. Hao et al., "Perspectives on optoelectronic oscillators," *APL Photonics* **8**(2), 020901 (2023).
12. X. S. Yao and L. Maleki, "Optoelectronic microwave oscillator," *J. Opt. Soc. Am. B* **13**(8), 1725–1735 (1996).
13. X. S. Yao and L. Maleki, "Converting light into spectrally pure microwave oscillation," *Opt. Lett.* **21**, 483–485 (1996).
14. D. Eliyahu, D. Seidel, and L. Maleki, "Phase noise of a high performance OEO and an ultra low noise floor cross-correlation microwave photonic homodyne system," in *IEEE Int. Freq. Control Symp.*, pp. 19–21 (2008).
15. X. S. Yao et al., "Dual-loop optoelectronic oscillator," in *Proc. IEEE Int. Freq. Control Symp.*, pp. 545–549 (1998).
16. X. S. Yao and L. Maleki, "Multiloop optoelectronic oscillator," *IEEE J. Quantum Electron.* **36**(1), 79–84 (2000).
17. S. Jia et al., "A novel optoelectronic oscillator based on wavelength multiplexing," *IEEE Photonics Technol. Lett.* **27**(2), 213–216 (2015).
18. X. S. Yao and L. Maleki, "Dual microwave and optical oscillator," *Opt. Lett.* **22**(24), 1867–1869 (1997).
19. X. S. Yao, L. Davis, and L. Maleki, "Coupled optoelectronic oscillators for generating both RF signal and optical pulses," *J. Lightwave Technol.* **18**(1), 73–78 (2000).
20. D. Zhu, T. H. Du, and S. L. Pan, "A coupled optoelectronic oscillator with performance improved by enhanced spatial hole

burning in an erbium-doped fiber," *J. Lightwave Technol.* **36**(17), 3726–3732 (2018).
21. K. Volyanskiy et al., "Compact optoelectronic microwave oscillators using ultra-high Q whispering gallery mode disk-resonators and phase modulation," *Opt. Express* **18**(21), 22358–22363 (2010).
22. D. Eliyahu et al., "Resonant widely tunable opto-electronic oscillator," *IEEE Photonics Technol. Lett.* **25**, 1535–1538 (2013).
23. K. H. Lee, J. Y. Kim, and W. Y. Choi, "Injection-locked hybrid optoelectronic oscillators for single-mode oscillation," *IEEE Photonics Technol. Lett.* **20**(19), 1645–1647 (2008).
24. A. Banerjee et al., "Analysis of injection locking and pulling in single-loop optoelectronic oscillator," *IEEE Trans. Microw. Theory* **67**(5), 2087–2094 (2019).
25. Z. Q. Fan et al., "Injection locking and pulling phenomena in an optoelectronic oscillator," *Opt. Express* **29**(3) 4681–4699 (2021).
26. P. Zhou et al., "Performance enhancement of an optically-injected-semiconductor-laser-based optoelectronic oscillator by subharmonic microwave modulation," *Opt. Lett.* **43**(21), 5439–5442 (2018).
27. J. J. Zhang et al., "Parity-time symmetry in wavelength space within a single spatial resonator," *Nat. Commun.* **11**, 3217 (2020).
28. H. Ding et al., "Observation of parity-time symmetry in time-division multiplexing pulsed optoelectronic oscillators within a single resonator," *Photonics Res.* **10**, 1915–1923 (2022).
29. Z. Dai et al., "Frequency-tunable parity-time-symmetric optoelectronic oscillator using a polarization-dependent Sagnac loop," *J. Lightwave Technol.* **38**, 5327–5332 (2020).
30. J. Fan et al., "A parity-time-symmetric optoelectronic oscillator based on non-reciprocal electro-optic modulation," *J. Lightwave Technol.* **39**(8), 2305–2310 (2021).
31. T. Hao et al., "Breaking the limitation of mode building time in an optoelectronic oscillator," *Nat. Commun.* **9**, 1839 (2018).
32. L. Wang et al., "Generation of reconfigurable linearly chirped microwave waveforms based on Fourier domain mode-locked optoelectronic oscillator," *J. Lightwave Technol.* **40**, 85–92 (2022).
33. B. Yang et al., "Active mode-locking optoelectronic oscillator," *Opt. Express* **28**(22), 33220–33227 (2020).
34. Z. Zeng et al., "Microwave pulse generation via employing an electric signal modulator to achieve time-domain mode locking in an optoelectronic oscillator," *Opt. Lett.* **46**(9), 2107–2110 (2021).
35. E. C. Levy and M. Horowitz, "Single-cycle radio-frequency pulse generation by an optoelectronic oscillator," *Opt. Express* **19**, 17599–17608 (2011).
36. E. C. Levy and M. Horowitz, "Theoretical and experimental study of passive mode-locked optoelectronic oscillators," *J. Opt. Soc. Am. B* **30**, 107–112 (2013).
37. T. Hao et al., "Optoelectronic parametric oscillator," *Light Sci. Appl.* **9**(1), 102 (2020).
38. Z. Ge et al., "Broadband random optoelectronic oscillator," *Nat. Commun.* **11**, 5724 (2020).
39. Z. Ge et al., "Tb/s fast random bit generation based on a broadband random optoelectronic oscillator," *IEEE Photonics Technol. Lett.* **33**(22), 1223–1226 (2021).
40. T. Hao et al., "Dissipative microwave photonic solitons in spontaneous frequency-hopping optoelectronic oscillators," *Photonics Res.* **10**(5), 1280–1289 (2022).
41. B. Romeira et al., "Broadband chaotic signals and breather oscillations in an optoelectronic oscillator incorporating a microwave photonic filter," *J. Lightwave Technol.* **32**(20), 3933–3942 (2014).
42. D. Ghosh et al., "Generation & control of chaos in a single loop optoelectronic oscillator," *Optik* **165**, 275–287 (2018).
43. J. Guo et al., "Graphdiyne-polymer nanocomposite as a broadband and robust saturable absorber for ultrafast photonics," *Laser Photonics Rev.* **14**(4), 1900367 (2020).
44. J. Guo et al., "Broadband nonlinear response and ultrafast photonics applications in few-layer MBene," *ACS Photonics* **10**(7), 2353–2362 (2023).

Hao Chen received his PhD in communication and information systems from Nanjing University of Aeronautics and Astronautics, Nanjing, China, in 2021. He is currently a research assistant at the Hangzhou Institute of Advanced Studies, Zhejiang Normal University, Hangzhou, China. His current research interests include photonic-microwave signal generation and fiber optic sensors.

Shifeng Liu received his MS and PhD degrees in physical electronics and communication and information systems in 2015 and 2022, respectively, from Nanjing University of Aeronautics and Astronautics, Nanjing, China. He has authored or co-authored more than 20 papers in peer-reviewed journals and 5 papers in conference proceedings. His research interests include ultra-low phase noise photonic-microwave signal generation, microwave photonic measurement, and high-performance radio-over-fiber systems.

Tongtong Xie is currently pursuing her PhD in the Department of Electronics Engineering, Xiamen University, Xiamen, China. Her current research interests include fiber optic sensing technology and signal generation technology based on microwave photonics.

Qingshui Guo received his MS degree in electronic science and technology from Nanjing University of Aeronautics and Astronautics, Nanjing, China, in 2018. He is currently a senior engineer at the Zhejiang Lab, Hangzhou, China. His current research interests include optical interconnects and microwave photonics.

Qiuyi Shen is currently working toward her MEng degree in electrical and information engineering at the Hangzhou Institute of Advanced Studies, Zhejiang Normal University, Hangzhou, China. Her research focuses on optoelectronic oscillators.

Chen Zhu received his PhD in electrical engineering from Missouri University of Science and Technology, Missouri, USA, in 2021. He is now working at the Research Center for Optical Fiber Sensing, Zhejiang Lab, Hangzhou, China. His research interest is focused on the development of fiber optic and microwave devices for sensing applications in harsh environments. He has authored or co-authored over 60 refereed articles, 20 conference papers, and 1 book chapter.

Daru Chen received his PhD from Zhejiang University, Hangzhou, China, in 2009. He is currently a professor in Hangzhou Institute of Advanced Studies, Zhejiang Normal University, Hangzhou, China. His current research interests include fiber lasers, fiber sensors, and photonic crystal fibers.

Hongyan Fu received her PhD in optical engineering from Zhejiang University, Hangzhou, China, in 2010. Currently, she is a professor in the Department of Electronic Engineering, Xiamen University, Xiamen, China. Her research interests include fiber optic sensors, fiber-based devices, and microwave photonics.

Shilong Pan received his PhD in electronic engineering from Tsinghua University, Beijing, China, in 2008. In 2010, he joined the College of Electronic and Information Engineering, Nanjing University of Aeronautics and Astronautics, Nanjing, China, where he is currently a full professor and the director of the National Key Laboratory of Microwave Photonics. His research focuses on optical generation and processing of microwave signals, analog photonic links, photonic microwave measurement, and integrated microwave photonics.